applied sciences

MDPI

*Article*

# Improved SPGD Algorithm for Optical Phased Array Phase Calibration

**Zheng Wang [1,2,†], Yibo Yang [1,2,†], Ruiting Wang [1,2], Guangzhen Luo [1,2], Pengfei Wang [1,2], Yanmei Su [1,2], Jiaoqing Pan [1,2] and Yejin Zhang [1,2,*]**

[1] State Key Laboratory on Integrated Optoelectronics, Institute of Semiconductors, Chinese Academy of Sciences, Beijing 100045, China
[2] Center of Materials Science and Optoelectronic Engineering, University of Chinese Academy of Sciences, Beijing 101408, China
* Correspondence: yjzhang@semi.ac.cn
† These authors contributed equally to this work and should be considered co-first authors.

**Abstract:** A chip-level optical beam steerer is an inevitable choice for next-generation light detection and ranging (LiDAR). The research on optical phased array (OPA) is the most intriguing. However, the complexity of control and calibration speed limit the full potential as the number of channels increases. In this paper, an improved stochastic parallel gradient-descent algorithm combined with the Nesterov accelerated gradient method (NSPGD) is presented and applied in a 512-channel OPA. This algorithm can reduce the phase calibration time of large-scale OPA and demonstrates a better convergence performance than traditional SPGD. Compared with the traditional SPGD and hill-climbing (HC) algorithm, optimized convergence performance of NSPGD is shown. The side mode suppression ratio (SMSR) of over 10dB for 512-channel OPA is obtained with the NSPGD algorithm, and the convergence speed is twice that of traditional SPGD. In addition, a temperature-controlled OPA is also studied to stabilize the whole calibration system.

**Keywords:** optical phased array; LiDAR; phase calibration algorithm; SPGD; temperature controlled OPA

**Citation:** Wang, Z.; Yang, Y.; Wang, R.; Luo, G.; Wang, P.; Su, Y.; Pan, J.; Zhang, Y. Improved-SPGD Algorithm for Optical Phased Array Phase Calibration. *Appl. Sci.* **2022**, *12*, 7879. https://doi.org/10.3390/app12157879

Academic Editor: Edik U. Rafailov

Received: 31 May 2022
Accepted: 4 August 2022
Published: 5 August 2022

**Publisher's Note:** MDPI stays neutral with regard to jurisdictional claims in published maps and institutional affiliations.



## 1. Introduction

Light detection and ranging (LiDAR) is a ranging technology to obtain 3D information from the outside world, which can be applied in industrial robots, augmented reality (AR), and advanced driver-assistance systems (ADAS). Optical phased array (OPA) is a fully solid solution for LiDAR, which is compatible with complementary metal oxide semiconductor (CMOS) technology and has become a research hotspot in recent years [1–10]. Ghent university reported the first 16-channel OPA based on silicon on insulator (SOI) in 2009 [1], with a field of view (FOV) of 14.1° × 2.3° and a beam width of 2.7° × 2.5°. Intel reported a 128-channel OPA with an 80° FOV in the phased-array axis and a 0.14° beam width in 2016 [2]. The University of Southern California demonstrated a 1024-channel OPA in 2018 [3], with a 0.03° beam width and a 45° FOV. Our previous works also reported some research results of OPA [11–14]. As we know, a large array with more channels that decreases beam width can improve the resolution of OPA. However, large arrays, especially those with thermal-optical modulators, can be influenced by the heat accumulation in addition to the process non-uniformity, which easily introduced phase error. In order to calibrate the phase error, many algorithms are proposed, such as the hill climbing (HC) algorithm [4], genetic algorithm (GA) [15] and stochastic parallel gradient descent (SPGD) [16]. However, the HC algorithm is difficult to calibrate for a large-scale OPA because it scans channel electrical signals one-by-one. Therefore, the time efficiency is too low. GA can be used to calibrate large-scale OPA, but its convergence

time is too long to be accepted. Xidian University calibrated a 64-channel OPA with SPGD. They collected light intensity with a high-speed photodetector (PD), which is a difficult-to-calibrate beam in when used on a large range because PD has to move while the scanning angle of OPA is changing. In addition, traditional SPGD easily falls into local extreme and the convergence speed is slow [17]. In this paper, an improved SPGD combined with Nesterov accelerated gradient (NAG)-NSPGD is proposed. A 512-channel OPA is optimized and calibrated successfully with a traditional InGaAs charge-coupled device (CCD) camera system. In addition, due to the application of a thermo-optic phase shifter, thermal accumulation is difficult to ignore; therefore, we introduce a temperature control structure to maintain stable thermal conditions. Based on our method, we can obtain the optimized OPA emission point, whose side mode suppression ratio (SMSR) is more than 10 dB, and the convergence speed is twice that of traditional SPGD.

## 2. OPA Characteristics and System Construction

In this work, a 512-channel OPA was used. By adjusting the wavelength and phase delay of the laser source, the beam could be controlled vertically and horizontally. The structure of our 512-channel OPA is like the 128-channel OPA described in reference [7]. The 128-channel OPA includes four parts: input coupler, optical beam splitter, thermos-optic phase shifter and optical antenna. The grating antenna is constructed on a wide silicon slab. The grating period is 470nm, the duty cycle is 50%, and the regular 70 nm shallow etching. A large two-dimensional FOV of 104° × 17.6° can be obtained. We also extend it to a 512-channel OPA, and it is tested by our phase calibration algorithm. More comprehensive experimental results of the 512-channel OPA will be reported in the future.

In order to evaluate the performance of our calibration algorithm, a system is built, as shown in Figure 1. The system consists of two parts: an electric circuit and an optical circuit. The electric circuit is used to transmit signals, feed algorithms, and control the phase difference between waveguides. The optical circuit is used to supply a laser source for OPA chips. Grating is sensitive to the polarization of light, so a polarization controller is installed in this system. The algorithm fitness function is the intensity of light emitted by the OPA chip from a reflection screen.

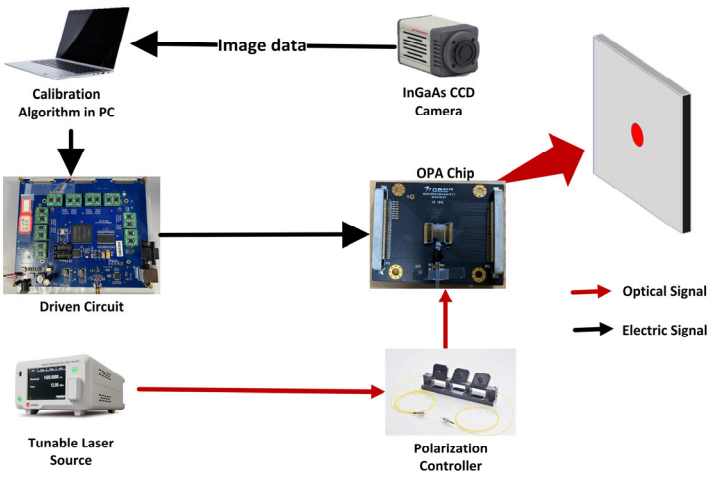


**Figure 1.** The phase calibration system of an OPA.

The calibration of phase difference between antennas mainly includes several steps. Firstly, the algorithm software works and sends signals to drive the circuit through the communication program. Then, the drive circuit converts the digital signals into analog ones and sends analog signals to phase shifters. After changing the voltage of phase shifters, the light intensity of the beam far-field will change accordingly, and CCD receives the light intensity integral information, which will be fed back to the control system. Then,

the algorithm process will be executed in specific logic, and the system will send the subsequent group signals to control the phase shifters. This cycle continues until the stop condition is met.

## 3. Calibrating Algorithm

SPGD is a popular adaptive wave-front control technique proposed by M. A. Vorontsov [18,19]. In the SPGD algorithm with *N* control channels, the fitness function is defined as

$$J = J\left(u_1,\ u_2,\ \ldots,\ u_N\right) \tag{1}$$

where $u_i$ is the voltage of the *i*th channel.

Random perturbations $\delta u_j$ , whose average value is 0 and variance is equal, i.e.,

$$< \delta u_i >= 0 \tag{2}$$

$$\delta u_i \delta u_j = \sigma^2 \delta_{ij} \tag{3}$$

Applying them to every channel simultaneously and

$$J^+ = J(\boldsymbol{u}+\delta\boldsymbol{u}) \tag{4}$$

$$J^- = J(\boldsymbol{u}\text{-}\delta\boldsymbol{u}) \tag{5}$$

$$\delta J = \frac{J^+ - J^-}{2} \tag{6}$$

Applying them to

$$u_j^{(k+1)} = u_j + \gamma \delta J^{(k)} \delta u_j^{(k)} \tag{7}$$

where *k* is the number of iterations, and $\gamma$ represents learning rate, which is one of the determining factors of $u_j$ . Renew the parameter $u$ and calculate the next iteration until the stop condition is satisfied.

However, traditional SPGD easily falls into the local optimum, and the convergence speed is limited [17].

NAG is a method that can endow gradient descent (GD) momentum [20,21], and improve GD's convergence performance. The basic equation of NAG is described as

$$m^{k+1} = \mu \cdot m^k + \gamma \cdot \nabla_\theta J(\theta - \mu \cdot m^k) \tag{8}$$

$$\theta^{k+1} = \theta^k - m^{k+1} \tag{9}$$

where $\mu \cdot m^k$ is the momentum term, $\mu$ is the momentum factor, $\gamma$ denotes the learning rate, $\theta$ denotes the current status (if in the OPA system, it represents the voltage of the channel),and $\nabla_\theta J$ is the partial derivative of the fitness function. $m^k$ is used to drive the movement of system status and $\theta - \mu \cdot m^k$ will predict the approximation of the status in the future.

Therefore, we combine NAG and SPGD to bring prediction into traditional SPGD. The combined equation is described as

$$m^{k+1} = \mu \cdot m^k + \gamma \cdot (\delta J - \mu \cdot m^k) \tag{10}$$

$$u_j^{k+1} = u_j^k - m^{k+1} \cdot \delta u_j^k \tag{11}$$

Fitness function in our system is defined as

$$J = \iint_{\Omega} I d\sigma \tag{12}$$

where $\Omega$ is the region chosen to integrate light intensity and $I$ represents the light intensity. The flow chart of the NSPGD algorithm is shown in Figure 2; firstly, some parameters such as $\gamma$, $k$, $\mu$, and $G$ are initialized, then $\delta u$ will be generated, $J^+$, $J^-$ and $\frac{J^+ - J^-}{2}$ are evaluated afterward. Momentum $m$ will be calculated, and these values are applied to Equation (11) and $J(u^{(k+1)})$ will be compared to $J(u^k)$, if $J(u^{(k+1)}) > J(u^k)$, $J_{\max} = J(u^{(k+1)})$, otherwise $J_{\max} = J(u^k)$. Then, compare $k+1$ with $G$ (maximum iterations set in initialization); if $k + 1 < G$, $k = k + 1$ and start up the next iteration, otherwise output $J_{\max}$ and end the algorithm. The optimal solution, i.e., a voltage set, can be found after $G$ iterations.

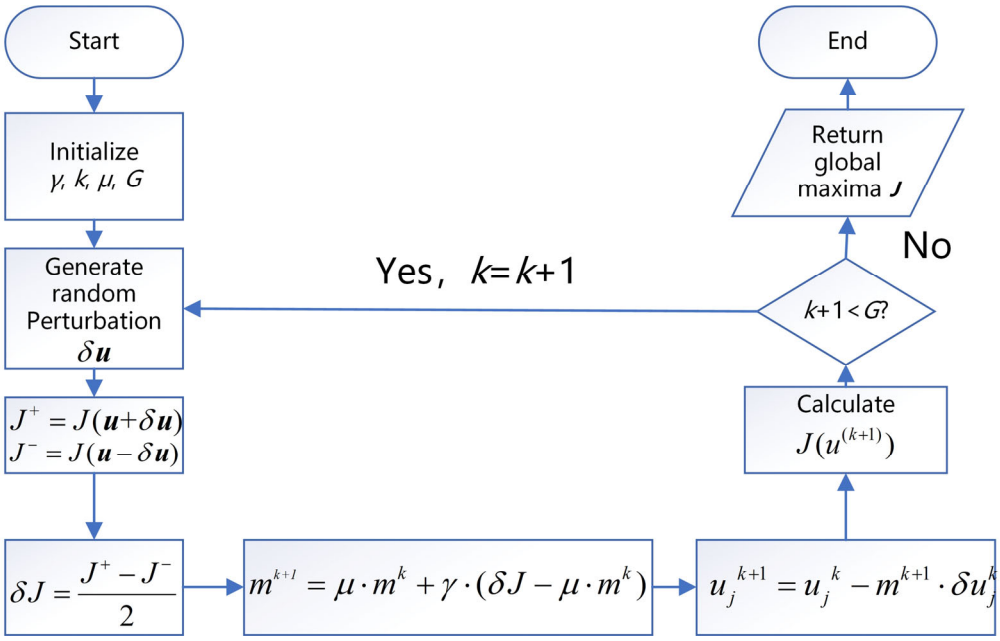


**Figure 2.** Flow chart of NSPDG algorithm.

We added the HC algorithm to the comparison to evaluate the performance of SPGD and NSPGD. How HC works is shown in Figure 3.

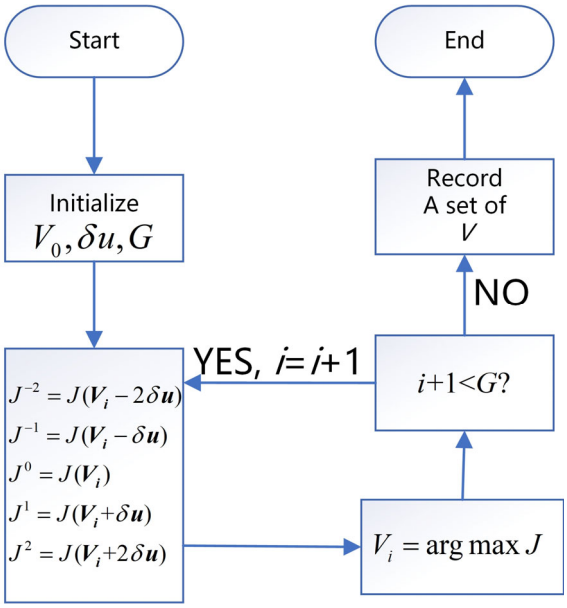


**Figure 3.** Flow chart of HC algorithm.

## 4. Experimental Results and Analysis

To test the performance of the improved SPGD mentioned in Section 3, NSPGD, SPGD, and HC algorithms are used to verify their performance. The performance is shown in Figure 4.

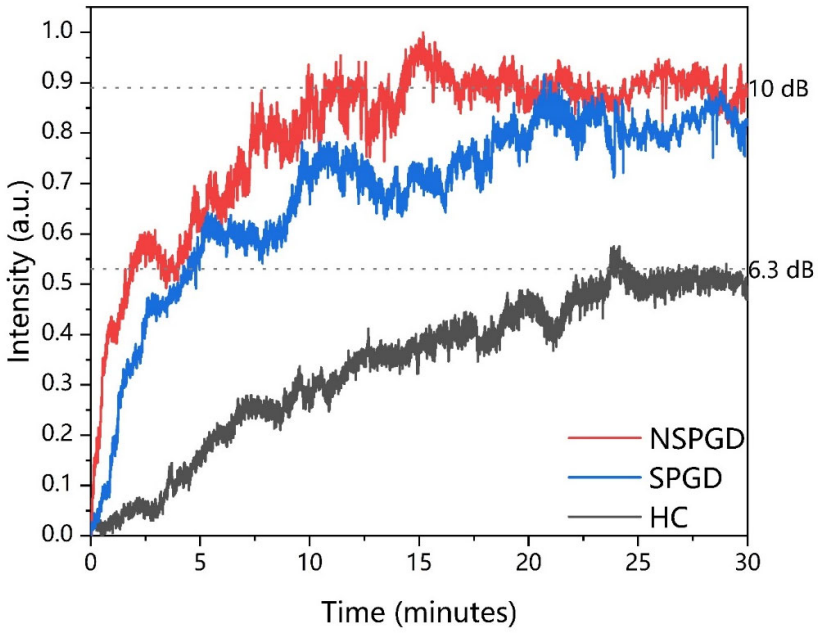


**Figure 4.** Convergence time of NSPGD, SPGD, and HC on 512-channel OPA.

As the convergence trend is shown in Figure 4, the NSPGD convergence rate is faster than that of SPGD and HC, and NSPGD takes about 10 min to over 10 dB while SPGD takes about 20 min. Furthermore, NSPGD converges to a better level (larger than 10 dB) than SPGD because it avoids the local maxima. It can be found that the convergence curve of NSPGD is more stable than SPGD, which can attribute to the momentum added to the

NSPGD. It has been proven that the momentum term can improve the performance of SPGD. After running for 30 min, only SMSR of 6.3 dB is obtained with HC method. This proves that NSPGD has good convergence performance.

Both thermo-optic (TO) and electro-optic (EO) phase shifters are applied in OPA widely [22–30]. Low loss can be obtained in TO shifters, while high power consumption and poor bandwidth follow. EO shifters hold high modulation up to GHz and low power consumption but induce extra loss because of the free carrier absorption effect. In order to ensure low loss, we use TO shifters in our OPA, which means watt level power concentrated in one $mm^2$ scale chip. Heat accumulation severely affects the chip's performance because Si is sensitive to temperature [31,32]. Many researchers tend to find ways to reduce the power consumption and thermal crosstalk to alleviate the adverse effect of heat brought by TO shifters [22,24,28]. One of the reasons for the performance degradation of OPA caused by TO shifters is that heat accumulation breaks the thermal equilibrium and makes the temperature around the waveguide unstable. So, some work attempts to conduct the heat to Si substrate [31–33], but they need an unconventional silicon process to grow material with high thermal conductivity.

Therefore, we designed a temperature-controlled packaging module shown in Figure 5. The OPA chip is bonded to the printed circuit board (PCB), and we cut a slot in the PCB to ensure good thermal contact. A thermistor is set between the thermoelectric cooler (TEC) to get the average temperature of the chip and TEC. The TEC is controlled by a proportional integral differential (PID) algorithm.

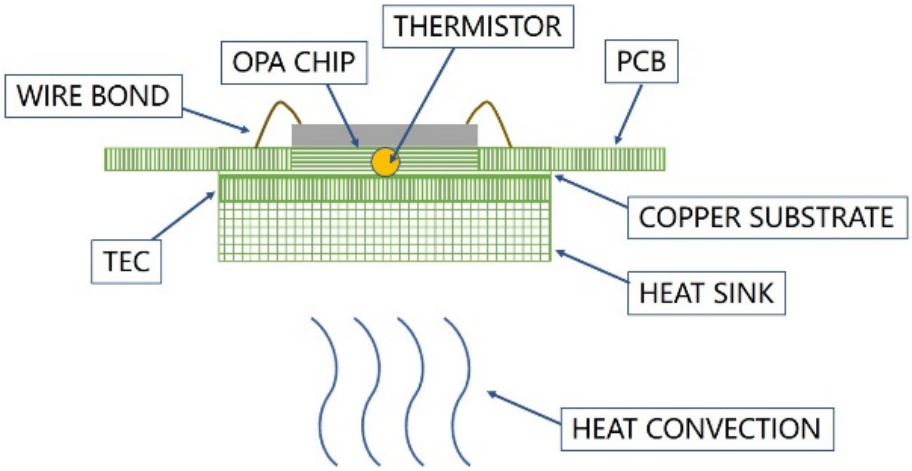


**Figure 5.** Schematic of 512-channel OPA with temperature-controlled packaging.

In order to test a 512-OPA with temperature-controlled packaging, 25 °C is set as the target temperature of the thermistor. The PID algorithm controls TEC to maintain a stable thermal environment. The influence of temperature control packaging on the convergence of the algorithm is verified by experiments. We applied NSPGD to the test. The convergence curve with temperature-controlled packaging meant that the target temperature of thermistor was set at 25 °C and the TEC worked to reach this goal. No temperature control means that the TEC is disabled and the heat accumulation is hard to dissipate. The results are shown in Figure 6, and was found that temperature control helps the algorithm converge better because it maintains a relatively stable environment for silicon waveguides and ensures it can only be impacted by TO shifters as much as possible. However, if temperature control is absent, there is a dynamic heat offset between the heat from TO shifters and heat accumulation, which may mess the algorithm up and hinder the convergence.

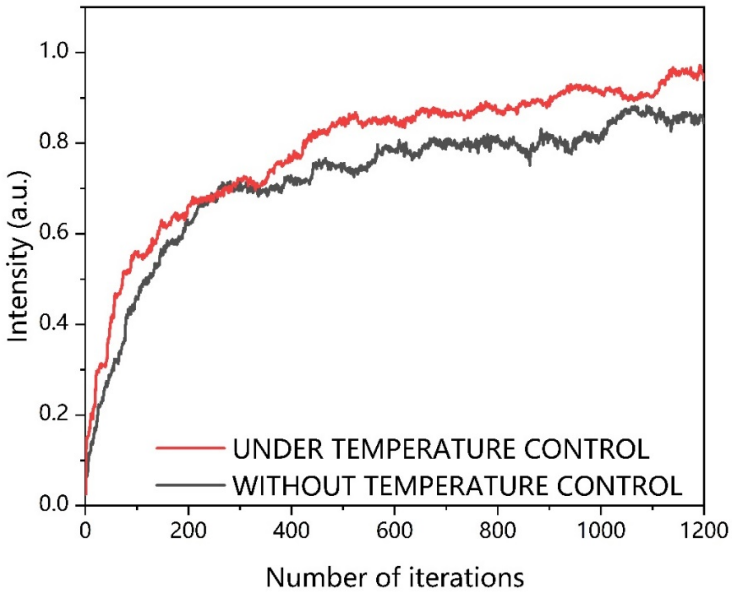


**Figure 6.** Convergence curve of under and without temperature control by NSPGD.

Temperature control helps obtain better calibration and saves calibration time. Repeated calibration will be implemented if the temperature control is absent because the room temperature and heat accumulation will change with time. Without temperature control and repeated calibration, up to 20% more (depending on room temperature variation) gray value degradation will be observed.

A set of voltages calibrated days ago are applied to the same OPA with our temperature-controlled packaging. The same main lobe beam will repeat.

Figure 7 shows the far-field 512-channel OPA calibrated by the NSPGD algorithm. The 512-channel OPA is successfully calibrated by NSPGD, and the SMSR is 10.4 dB. Compared with the initial beam, the side lobe is suppressed and the main lobe is optimized.

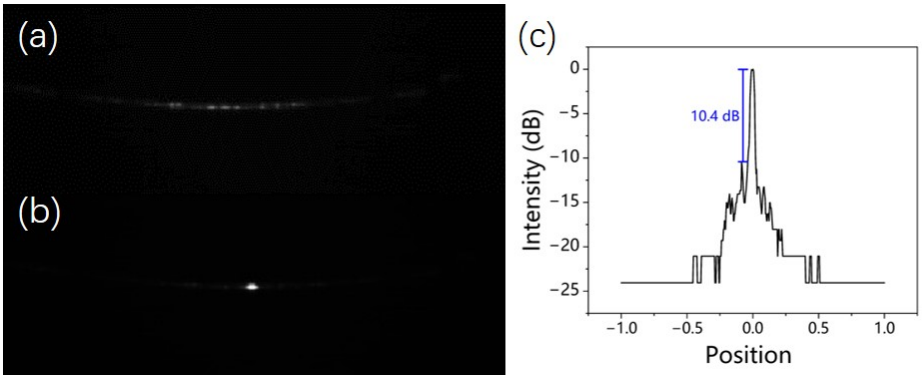


**Figure 7.** The 512-channel OPA (**a**) far-field without calibration, (**b**) far-field with NSPGD calibration, and (**c**) SMSR of far-field after calibration.

Finally, we calibrated the beam at different angles, and the results are shown in Figure 8. According to the change of selected $\Omega$ in our PC program, as described in Equation (12), the calibrated beams of different angles were obtained. $\Delta\varphi$ means the phase difference between adjacent emitters. Grating lobes will emerge with the scanning angle increasing because the distance between adjacent emitters is larger than $\lambda/2$. The beam in the red rectangle is the main lobe, and the side lobe locates in the white one.

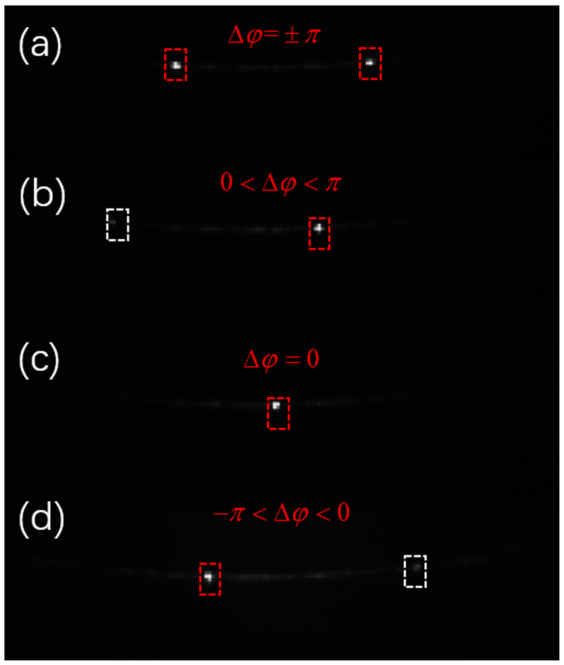


**Figure 8.** OPA beam with different phase differences (**a**) $\Delta\varphi=\pm\pi$, (**b**) $0<\Delta\varphi<\pi$, (**c**) $\Delta\varphi=0$, and (**d**) $-\pi<\Delta\varphi<0$.

## 5. Conclusions

An NSPGD algorithm and temperature-controlled packaging were proposed to improve calibration. A 512-channel OPA was tested to compare the convergence performance among NSPGD, SPGD, and HC. It was proven that the convergence performance of NSPGD is better than the others. An SMSR of over 10 dB for 512-channel OPA was observed with the calibration of NSPGD, and the convergence speed is twice that of traditional SPGD. The temperature-controlled packaging can help the algorithm converge better and avoid repeated calibration. The NSPGD and the temperature-controlled packaging can be extended to similar systems.

**Author Contributions:** Conceptualization, Y.Y.; Data curation, Z.W. and Y.S.; Formal analysis, G.L.; Methodology, P.W.; Project administration, J.P.; Software, R.W.; Writing—original draft, Z.W.; Writing—review and editing, Y.Z. All authors have read and agreed to the published version of the manuscript.

**Funding:** This work is supported by Natural Science Foundation of China (62090053, 61934007), Beijing Natural Science Foundation (Z200006, 4222078), National Key R&D Program of China (2018YFE0203103, 2021YFB2800304).

**Institutional Review Board Statement:** Not applicable.

**Informed Consent Statement:** Not applicable.

**Data Availability Statement:** Not applicable.

**Conflicts of Interest:** The authors declare no conflict of interest.

## References

1. Van Acoleyen, K.; Bogaerts, W.; Jágerská, J.; Le Thomas, N.; Houdré, R.; Baets, R. Off-chip beam steering with a one-dimensional optical phased array on silicon-on-insulator. *Opt. Lett.* **2009**, *34*, 1477–1479. https://doi.org/10.1364/OL.34.001477.
2. Hutchison, D.N.; Sun, J.; Doylend, J.K.; Kumar, R.; Heck, J.; Kim, W.; Phare, C.T.; Feshali, A.; Rong, H. High-resolution aliasing-free optical beam steering. *Optica* **2016**, *3*, 887–890. https://doi.org/10.1364/OPTICA.3.000887.
3. Chung, S.; Abediasl, H.; Hashemi, H. A monolithically integrated large-scale optical phased array in silicon-on-insulator CMOS. *IEEE J. Solid-State Circuits* **2017**, *53*, 275–296. https://doi.org/10.1109/JSSC.2017.2757009.

4. Doylend, K.J.; Heck, M.J.R.; Bovington, J.T.; Peters, J.D.; Coldren, L.A.; Bowers, J.E. Two-Dimensional Free-Space Beam Steering with an Optical Phased Array on Silicon-on-Insulator. *Opt. Express* **2011**, *19*, 21595–21604.
5. Sun, J.; Timurdogan, E.; Yaacobi, A.; Hosseini, E.S.; Watts, M.R. Large-Scale Nanophotonic Phased Array. *Nature* **2013**, *493*, 195–199.
6. Zhang, L.; Wang, Y.; Hou, Y.; Song, J. Uniform Rectangular Distribution of Far-Field Intensity by Optical Phased Array. *Opt. Commun.* **2021**, *509*, 127661.
7. Li, Y.; Chen, B.; Na, Q.; Xie, Q.; Tao, M.; Zhang, L.; Zhi, Z.; Li, Y.; Liu, X.; Luo, X.; et al. Wide-Steering-Angle High-Resolution Optical Phased Array. *Photonics Res.* **2021**, *9*, 2511–2518.
8. Zhang, L.; Li, Y.; Hou, Y.; Wang, Y.; Tao, M.; Chen, B.; Na, Q.; Li, Y.; Zhi, Z.; Liu, X.; et al. Investigation and Demonstration of a High-Power Handling and Large-Range Steering Optical Phased Array Chip. *Opt. Express* **2021**, *29*, 29755–29765.
9. Chen, B.; Li, Y.; Zhang, L.; Li, Y.; Liu, X.; Tao, M.; Hou, Y.; Tang, H.; Zhi, Z.; Gao, F.; et al. Unidirectional Large-Scale Waveguide Grating with Uniform Radiation for Optical Phased Array. *Opt. Express* **2021**, *29*, 20995–21010.
10. Xu, W.; Zhou, L.; Lu, L.; Chen, J. Aliasing-Free Optical Phased Array Beam-Steering with a Plateau Envelope. *Opt. Express* **2019**, *27*, 3354–3368.
11. Wang, P.; Luo, G.; Li, Y.; Yang, W.; Yu, H.; Zhou, X.; Zhang, Y.; Pan, J. Large scanning range optical phased array with a compact and simple optical antenna. *Microelectron. Eng.* **2020**, *224*, 111237. https://doi.org/10.1016/j.mee.2020.111237.
12. Wang, P.; Luo, G.; Xu, Y.; Li, Y.; Su, Y.; Ma, J.; Wang, R.; Yang, Z.; Zhou, X.; Zhang, Y.; et al. Design and fabrication of a SiN-Si dual-layer optical phased array chip. *Photonics Res.* **2020**, *8*, 912–919. https://doi.org/10.1364/PRJ.387376.
13. Ma, P.; Luo, G.; Wang, P.; Ma, J.; Wang, R.; Yang, Z.; Zhou, X.; Zhang, Y.; Pan, J. Unidirectional SiN antenna based on dual-layer gratings for LiDAR with optical phased array. *Opt. Commun.* **2021**, *501*, 127361. https://doi.org/10.1016/j.optcom.2021.127361.
14. Luo, G.; Wang, P.; Ma, J.; Wang, R.; Yang, Z.; Xu, Y.; Yu, H.; Zhou, X.; Zhang, Y.; Pan, J. Demonstration of 128-channel Optical Phased Array With Large Scanning Range. *IEEE Photonics J.* **2021**, *13*, 6800710. https://doi.org/10.1109/jphot.2021.3071185.
15. Liu, Q.; Lu, Y.; Wu, B.; Jiang, P.; Cao, R.; Feng, J.; Guo, J.; Jin, L. Silicon Optical Phased Array Side Lobe Suppression Based on an Improved Genetic Algorithm. In Proceedings of the 2020 Asia Communications and Photonics Conference (ACP) and International Conference on Information Photonics and Optical Communications (IPOC), Beijing, China, 24–27 October 2020; pp. 1–3.
16. Wang, X.C.Y.; Liu, C.; Zhao, X.; Chen, J.; Han, X.; Shi, Y. Phase Noise Compensation of Silicon-Based Optical Phased Array Chip. *Acta Opt. Sin.* **2021**, *41*, 2323001. https://doi.org/10.3788/aos202141.2323001.
17. Zhang, W.; Li, L.; Chen, W. A chaotic stochastic parallel gradient descent algorithm for fast phase correction of optical phased array. In Proceedings of the Eleventh International Conference on Information Optics and Photonics (CIOP 2019), Xi'an, China, 6–9 August 2019.
18. Vorontsov, M.A.; Carhart, G.W.; Ricklin, J.C. Adaptive phase-distortion correction based on parallel gradient-descent optimization. *Opt. Lett.* **1997**, *22*, 907–909. https://doi.org/10.1364/OL.22.000907.
19. Vorontsov, M.A. Decoupled stochastic parallel gradient descent optimization for adaptive optics: Integrated approach for wavefront sensor information fusion. *JOSA A* **2002**, *19*, 356–368. https://doi.org/10.1364/JOSAA.19.000356.
20. Nesterov, Y. A method for unconstrained convex minimization problem with the rate of convergence o(1/k^2). *Dokl. AN USSR* **1983**, *269*, 543–547.
21. Sutskever, I.; Martens, J.; Dahl, G.; Hinton, G. On the importance of initialization and momentum in deep learning. In Proceedings of the International Conference on Machine Learning, Atlanta, GA, USA, 16–21 June 2013; pp. 1139–1147.
22. Alemany, R.; Muñoz, P.; Pastor, D.; Domínguez, C. Thermo-Optic Phase Tuners Analysis and Design for Process Modules on a Silicon Nitride Platform. *Photonics* **2021**, *8*, 496.
23. Harris, N.C.; Ma, Y.; Mower, J.; Baehr-Jones, T.; Englund, D.; Hochberg, M.; Galland, C. Efficient, compact and low loss thermo-optic phase shifter in silicon. *Opt. Express* **2014**, *22*, 10487–10493. https://doi.org/10.1364/OE.22.010487.
24. Jacques, M.; Samani, A.; El-Fiky, E.; Patel, D.; Xing, Z.; Plant, D.V. Optimization of thermo-optic phase-shifter design and mitigation of thermal crosstalk on the SOI platform. *Opt. Express* **2019**, *27*, 10456–10471. https://doi.org/10.1364/OE.27.010456.
25. Poulton, C.V.; Russo, P.; Timurdogan, E.; Whitson, M.; Byrd, M.J.; Hosseini, E.; Moss, B.; Su, Z.; Vermeulen, D.; Watts, M.R. High-performance integrated optical phased arrays for chip-scale beam steering and lidar. In Proceedings of the CLEO: Applications and Technology, San Jose, CA, USA, 13–18 May 2018; p. ATu3R.2.
26. Rahim, A.; Hermans, A.; Wohlfeil, B.; Petousi, D.; Kuyken, B.; Van Thourhout, D.; Baets, R. Taking silicon photonics modulators to a higher performance level: State-of-the-art and a review of new technologies. *Adv. Photonics* **2021**, *3*, 024003.
27. Shi, P.; Lu, L.; Liu, C.; Zhou, G.; Xu, W.; Chen, J.; Zhou, L. Optical FMCW Signal Generation Using a Silicon Dual-Parallel Mach-Zehnder Modulator. *IEEE Photonics Technol. Lett.* **2021**, *33*, 301–304. https://doi.org/10.1109/LPT.2021.3057986.
28. Song, J.; Fang, Q.; Tao, S.H.; Liow, T.Y.; Yu, M.B.; Lo, G.Q.; Kwong, D.L. Fast and low power Michelson interferometer thermo-optical switch on SOI. *Opt. Express* **2008**, *16*, 15304–15311. https://doi.org/10.1364/OE.16.015304.
29. Xia, P.; Yu, H.; Zhang, Q.; Fu, Z.; Wang, X.; Wang, Y.; Jiang, X.; Yang, J. A Silicon Optical Single Sideband Modulator With Ultra-High Sideband Suppression Ratio. *IEEE Photonics Technol. Lett.* **2020**, *32*, 963–966. https://doi.org/10.1109/lpt.2020.3006468.
30. Zhang, Z.; Huang, Q.; Zhou, Z.; Wang, Y.; Yu, H.; Yang, J. Silicon Optical Phased Array Based on Carrier-depletion Phase Shifters. In Proceedings of the 2021 Asia Communications and Photonics Conference (ACP), Shanghai, China, 24–27 October 2021; pp. 1–2.

31. Krochin-Yepez, P.-A.; Scholz, U.; Zimmermann, A. CMOS-Compatible Measures for Thermal Management of Phase-Sensitive Silicon Photonic Systems. *Photonics* **2020**, *7*, 6.
32. Yepez, P.A.K.; Scholz, U.; Caspers, J.N.; Zimmermann, A. Novel Measures for Thermal Management of Silicon Photonic Optical Phased Arrays. *IEEE Photonics J.* **2019**, *11*, 6602415. https://doi.org/10.1109/JPHOT.2019.2925138.
33. Yepez, P.A.K.; Scholz, U.; Zimmermann, A. Temperature Dependence of the Steering Angles of a Silicon Photonic Optical Phased Array. *IEEE Photonics J.* **2020**, *12*, 6800813. https://doi.org/10.1109/JPHOT.2020.2966618.